

## Cenozoic plate boundary evolution in the South Island of New Zealand: New thermochronological constraints

Geoffrey E. Batt,<sup>1,2</sup> Suzanne L. Baldwin,<sup>3</sup> Michael A. Cottam,<sup>1</sup> Paul G. Fitzgerald,<sup>3</sup> Mark T. Brandon,<sup>4</sup> and Terry L. Spell<sup>5</sup>

Received 27 March 2003; revised 9 October 2003; accepted 16 April 2004; published 2 July 2004.

[1] Thermochronological investigations of samples collected west of the Alpine Fault zone provide new insight into the early development of the Australian-Pacific (AUS-PAC) plate boundary through New Zealand that is not preserved elsewhere in the modern orogenic system of the South Island. The  $^{40}\text{Ar}/^{39}\text{Ar}$ , fission track, and (U-Th)/He ages for these samples span the Cenozoic and provide direct constraints on the timing and character of two discrete episodes in the evolution of this tectonic boundary. The initial propagation of the AUS-PAC boundary through the South Island in the early Miocene is expressed as short-lived, geographically localized cooling, which we infer to be due to exhumation, beginning at 23–25 Ma. This is consistent with development of this boundary as an initially distributed zone of deformation, progressively localizing onto discrete fault structures developing primacy of strain accommodation over time. Regionally synchronous development of rapid cooling at 8 Ma corroborates the association of the present obliquely convergent character of the AUS-PAC boundary through the South Island with a marked change in Pacific plate motion at that time. Subsequent increases in cooling rate and a regionally prominent 5 Ma thermochronologic signal illuminate the progressive adaptation of the plate boundary to this new tectonic system over a period of  $\sim 3$  Myr, culminating in development of the extant tectonic regime.

**INDEX TERMS:** 1035 Geochemistry: Geochronology; 8102 Tectonophysics: Continental contractional orogenic belts; 8107 Tectonophysics: Continental neotectonics; 8150 Tectonophysics: Plate boundary—general (3040); 8158 Tectonophysics: Plate motions—present and recent (3040); **KEYWORDS:** Southern Alps, Alpine Fault, tectonic evolution,

argon, thermochronology, Australian-Pacific plate. **Citation:** Batt, G. E., S. L. Baldwin, M. Cottam, P. G. Fitzgerald, M. T. Brandon, and T. L. Spell (2004), Cenozoic plate boundary evolution in the South Island of New Zealand: New thermochronological constraints, *Tectonics*, 23, TC4001, doi:10.1029/2003TC001527.

### 1. Introduction

[2] The South Island of New Zealand is subject to ongoing oblique continent-continent convergence between the Australian and Pacific plates [Molnar *et al.*, 1975; Walcott, 1978, 1998; Allis, 1986; DeMets *et al.*, 1990; Norris *et al.*, 1990; Pearson *et al.*, 1995]. Associated uplift and deformation along the plate boundary has given rise to the Southern Alps, a prominent mountain range running much of the length of the island (Figure 1). The tectonic history of this orogenic system, and especially the initiation of the present phase of oblique convergence, is of considerable global interest, as the changes in plate motion responsible for this development have also been linked to other late Neogene events around the Pacific, including the onset of Pliocene compression along the San Andreas Fault [e.g., Pollitz, 1986; Harbert, 1991; Kamp, 1991; Atwater and Stock, 1998].

[3] As with many eroded orogenic regions, isotopic dating has long been used to quantitatively constrain the evolution of the Southern Alps [e.g., Adams and Gabites, 1985; Rattenbury, 1987; Kamp *et al.*, 1989, 1992; Tippett and Kamp, 1993; Chamberlain *et al.*, 1995; Kamp, 1997; Batt *et al.*, 2000; Batt, 2001]. Most recent investigations of this type have focused on the Pacific plate hanging wall of the Alpine Fault [e.g., Adams and Gabites, 1985; Tippett and Kamp, 1993; Chamberlain *et al.*, 1995; Batt *et al.*, 2000; Batt, 2001], where deep and rapid exhumation caused by the ongoing orogenesis has produced a strong thermochronologic signal [Tippett and Kamp, 1993; Shi *et al.*, 1996; Batt and Braun, 1999]. These studies are unable to provide great insight into the early evolution of the orogen, however, because of the extent of Pliocene-Recent convergence and exhumation along the Alpine Fault through the South Island (Figure 1c) removing rocks that recorded this early development [Beaumont *et al.*, 1996; Walcott, 1998; Batt and Brandon, 2002]. Following White and Green [1986], Seward [1989], and Kamp *et al.* [1992], we provide more detailed constraints on the thermal evolution of the less deformed and denuded Australian plate side of the AUS-PAC boundary zone, and reinterpret existing models of the developmental timeframe for the AUS-PAC system through the region. Although the Aus-

<sup>1</sup>Geology Department, Royal Holloway University of London, Surrey, UK.

<sup>2</sup>Formerly at the Department of Geology and Geophysics, Yale University, New Haven, Connecticut, USA.

<sup>3</sup>Department of Earth Sciences, Syracuse University, Syracuse, New York, USA.

<sup>4</sup>Department of Geology and Geophysics, Yale University, New Haven, Connecticut, USA.

<sup>5</sup>Department of Geoscience, University of Nevada, Las Vegas, Nevada, USA.

tralian plate may also have experienced destructive overthrusting during early stages of the Pliocene-Recent oblique convergence [Sutherland *et al.*, 2000], it preserves a more detailed record of progressive Cenozoic development of the plate boundary [White and Green, 1986; Seward, 1989; Kamp *et al.*, 1992], as thermal weakening and focus of strain along the uplifted Pacific plate side of

the Alpine Fault rapidly assumed primacy in this system [Koons *et al.*, 2003].

[4] Whereas White and Green [1986], Seward [1989], and Kamp *et al.* [1992] derive their interpretations from spatial trends in fission track and other geologic data integrated across a wide geographical range, we integrate a variety of thermochronologic data to provide a set of

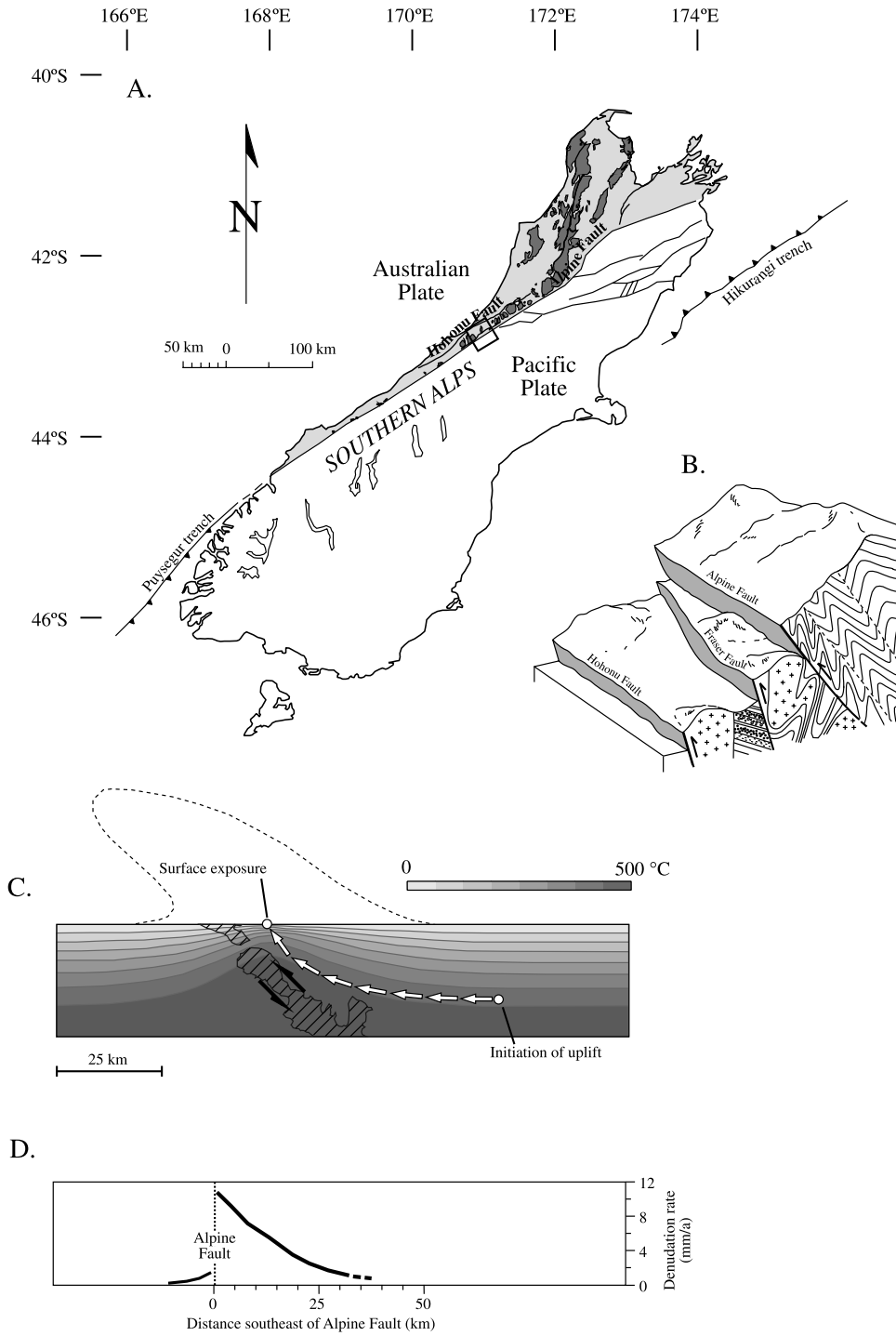


Figure 1

robust, internally consistent thermal histories for individual samples from different localities west of the Alpine Fault.

[5] The principal tool we apply is the  $^{40}\text{Ar}/^{39}\text{Ar}$  K-feldspar multidiffusion domain (MDD) modeling approach, which provides direct constraint of the thermal sensitivity of each individual sample [Lovera *et al.*, 1991]. This is complemented by higher temperature  $^{40}\text{Ar}/^{39}\text{Ar}$  mica data and low temperature constraints from apatite fission track and apatite (U-Th)/He data. By developing such spatially discrete thermal histories for samples collected as close as practical to the Alpine Fault along the West Coast, our objective was to isolate the signal of tectonic change through time at this plate boundary, and distinguish it from diachronous spatial variation in deformation of the wider orogenic system [e.g., Stüwe *et al.*, 1994; Jamieson *et al.*, 1996; Harrison *et al.*, 1998; Batt and Brandon, 2002].

## 2. Regional Geology

[6] The West Coast region borders much of the western side of New Zealand's South Island, broadening from a coastal strip 10–20 km across in the south to over 100 km wide in the north (Figure 1). Although subdued in comparison to the Southern Alps immediately to the east, the West Coast is topographically rugged in its own right, rising from sea level to approximately 1000 m elevation. The region is largely underlain by rocks of continental affinity [Nathan *et al.*, 1986], which can be subdivided into three major units - the Charleston Metamorphic Group, early Paleozoic meta-sediments, and a varied suite of intrusive rocks.

[7] Granites related to major periods of intrusion in the Devonian, Carboniferous, and Cretaceous [Kimbrough and Tulloch, 1989; Seward, 1989; Muir *et al.*, 1994, 1996] are widespread throughout the West Coast, underlie much of the high topography in the north (Figure 1), and form a series of prominent isolated mountains and hills west of the Alpine Fault [Reed, 1958; Tulloch, 1983]. Granitic bodies discordantly intrude both the Charleston Metamorphic Group [Shelley, 1970; Nathan, 1975, 1978] and the Paleozoic sediments of the West Coast [Cooper, 1979; Cooper and Grindley, 1982], and have locally induced contact metamorphism in the latter [Nathan *et al.*, 1986].

[8] A distinctive narrow sliver of higher-grade midcrustal rocks occurs in the central West Coast (Figures 1b and 2). These comprise a complex association of midgreenschist facies mylonites anastomosing around less deformed lenses of granite and gneiss up to several kilometers in size, and are collectively referred to as the Fraser Complex [Rattenbury, 1987]. Bounded by the Alpine Fault to the east and Fraser Fault to the west, the structural complexity and fault-truncated nature of these rocks leaves their wider lithological affinity ambiguous.

## 3. Tectonic Setting

[9] The modern Alpine Fault Zone represents the boundary between the Australian and Pacific plates through the central South Island, separating the West Coast region of Australian plate affinity from the Pacific plate material making up the Southern Alps to the east. This structural zone is traceable in reflection and refraction seismic surveys to depths of at least 25 km [Smith *et al.*, 1995; Davey *et al.*, 1995] and, at a regional scale, accommodates both the normal and transverse components of relative Australian-Pacific plate motion [Norris *et al.*, 1990], with movement on the Alpine Fault accounting for an estimated 60 to 90% of the total relative AUS-PAC plate velocity [e.g., Sutherland, 1994; Norris and Cooper, 2001].

[10] The Alpine Fault initially propagated through the South Island as a transform structure linking the Hikurangi and Puysegur subduction zones during the latest Oligocene to early Miocene, exploiting the preexisting fabric of Eocene-Oligocene basins across western New Zealand [Molnar *et al.*, 1975; Carter and Norris, 1976; Kamp, 1986; Cooper *et al.*, 1987; King, 2000; Sutherland *et al.*, 2000]. Early movement along the proto-Alpine Fault saw the Eocene-Miocene passive margin and oceanic crust adjoining the Pacific plate overridden by the Pacific plate [Sutherland *et al.*, 2000], juxtaposing continental rocks either side of the AUS-PAC boundary.

[11] The present obliquely convergent dynamics of the South Island of New Zealand developed during the Pliocene owing to a major shift in the instantaneous Euler pole for Australian-Pacific motion to the southwest [Walcott, 1984;

**Figure 1.** (a) Major geological features of the AUS-PAC plate boundary through the South Island and the West Coast. The West Coast region as a whole is shaded light gray, with exposures of granitic rocks indicated by darker shading. Rectangular frame inset across the Alpine and Hohonu Faults indicates the approximate location of the block diagram shown in Figure 1b. (b) Schematic block diagram summarizing geological variation across the West Coast and major fault structures through the region. This is a composite diagram, drawing on the results of Reyners and Cowan [1993], Smith *et al.* [1995], Rattenbury [1987], and Kamp *et al.* [1992], and is not drawn to scale, intending only to show the relative structural and lithological relationship of the key components of the West Coast system. (c) Numerical model results illustrating the exhumation history of a particle passing through a convergent orogenic system modeled on the Southern Alps, after Batt [1997] and Batt and Braun [1997, 1999]. Convergence is at 10 mm/yr, horizontal and vertical scales are equal, and the thermal structure shown is that developed after 5 Myr of deformation. The crosshatched region marks the peak strain rates in the model after 5 Myr, and is interpreted to equate with the Alpine Fault for the Southern Alps (Figure 1b). The open arrows show the exhumation trajectory of a selected particle, and the dashed envelope above the modeled orogen represents the approximate volume of eroded material lost from the system during evolution of the model. (d) Approximate exhumation rates across the central Southern Alps, drawing together the fission track dating results of Kamp *et al.* [1992] and Tippett and Kamp [1993]. Rates are plotted relative to the Alpine Fault, with the same horizontal scale as in Figure 1c, to allow direct comparison between the two panels.

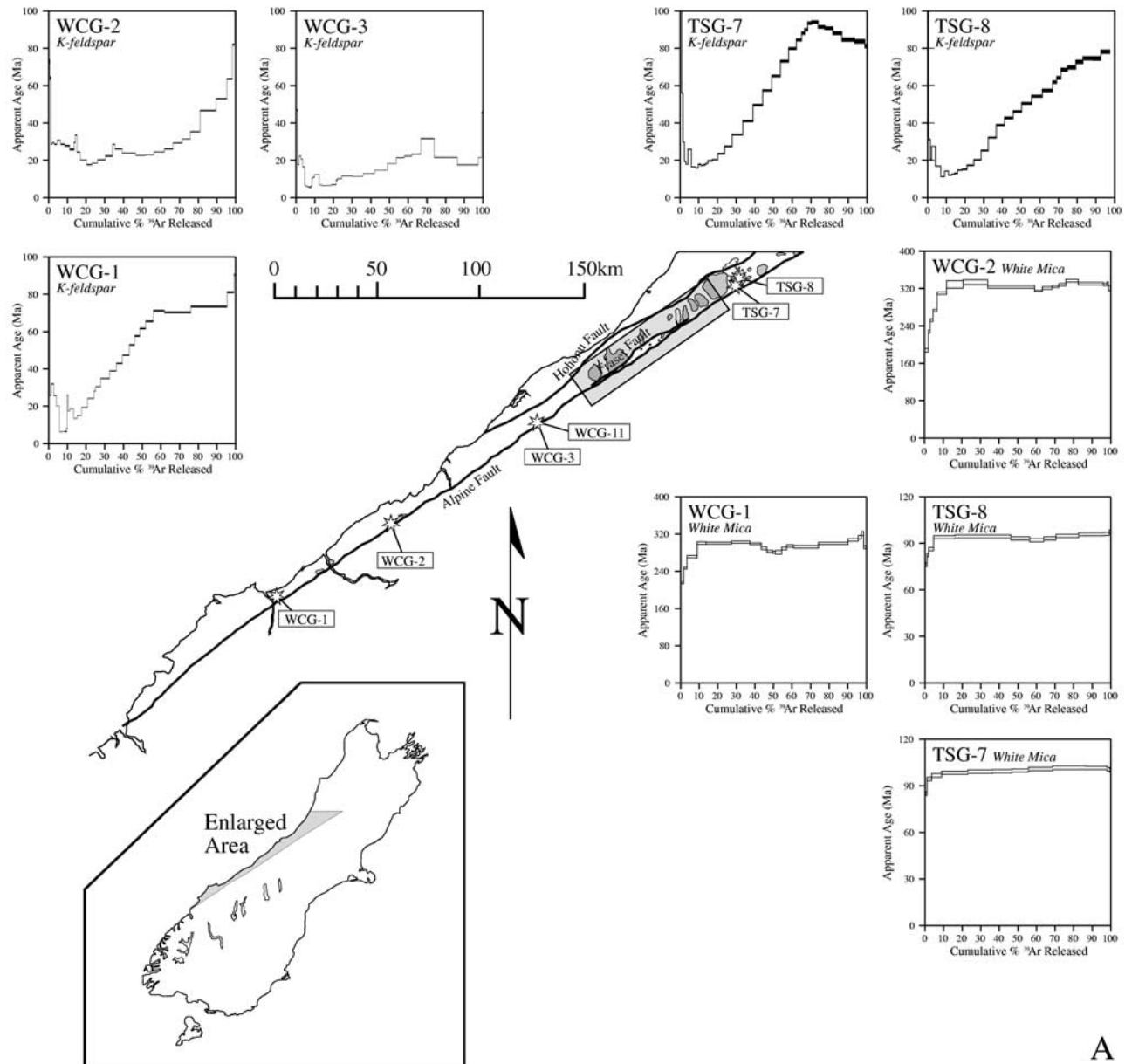


**Figure 2.** Distribution of samples and basic chronological data collected in this study. The  $^{40}\text{Ar}/^{39}\text{Ar}$  age spectra are constructed by plotting the apparent  $^{40}\text{Ar}/^{39}\text{Ar}$  age of gas released against the cumulative percentage of  $^{39}\text{Ar}$  released during heating. The amount of  $^{39}\text{Ar}$  released in each heating step is indicated by the width of each discrete segment of the illustrated spectrum. For more information on the detail of the heating schedule of experiments and raw data, full data tables are available in the auxiliary material to this work<sup>1</sup>. Elongate shaded box in Figure 2a highlights the area enlarged in Figure 2b to illustrate the structural detail of the closely spaced sample localities from around the northern end of the Fraser Complex.

*Sutherland, 1995; Walcott, 1998*], possibly driven by slab break-off beneath the margin of the Pacific plate [e.g., *Cox and Engebretson, 1985*]. Oblique AUS-PAC convergence since  $\sim 8.3$  Ma [*Kamp et al., 1992*] has produced minor

distributed reverse faulting and thickening throughout the West Coast region [*Nathan et al., 1986; Seward, 1989; Kamp et al., 1992, 1996*], at an order of magnitude lower rates and intensity than the ongoing deformation experienced in the Pacific plate to the east. Accompanying erosion has stripped the relatively soft former Cretaceous-Cenozoic cover rocks from the ranges [*Seward, 1989*], while com-

<sup>1</sup>Auxiliary material is available at <ftp://ftp.agu.org/apend/tc/2003TC001527>.

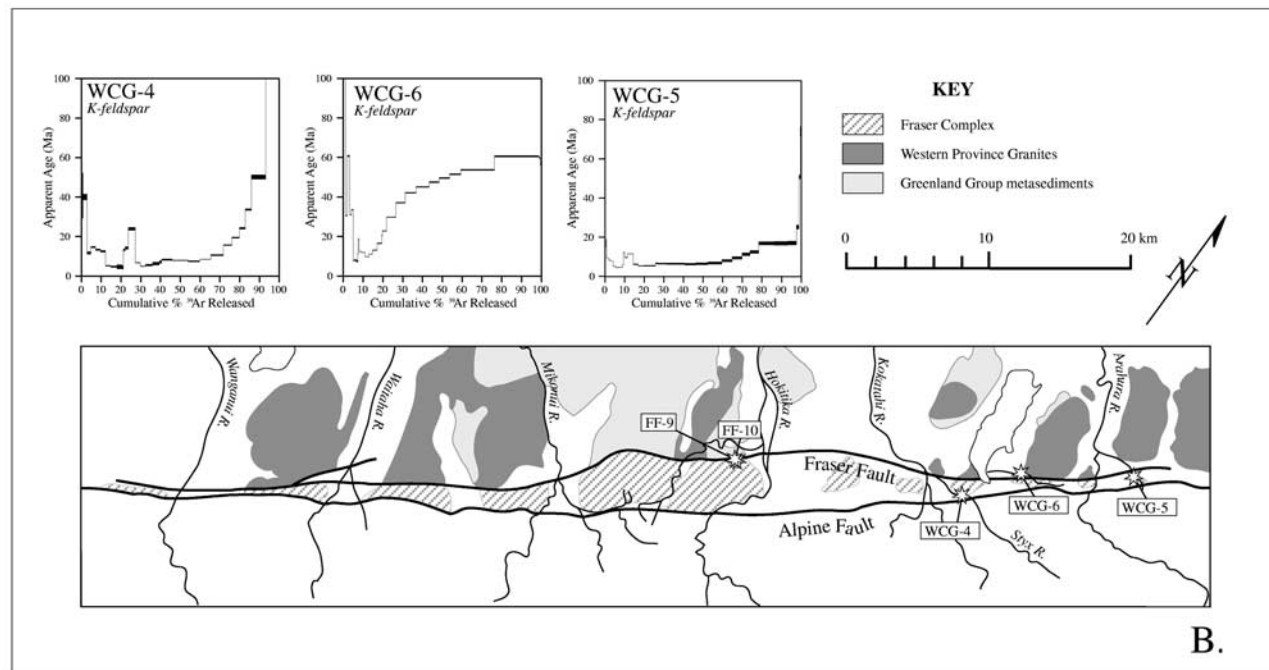


Figure 2. (continued)

monly leaving these sediments preserved as thick deformed sequences in the intervening basins.

#### 4. Analytical Procedures

[12] A suite of samples, largely granitic in composition, and ranging from undeformed to gneissic in character, was collected from localities proximal to the Alpine Fault zone (Figure 2 and Table 1) between McPherson's Creek in the north and the Arawhata River in the south. After petrographic assessment of mineral content, high purity (>99%) separates of K-feldspar were prepared from crushed and sieved rock chips by Donelick Analytical Inc. (now Apatite to Zircon, Inc.) using conventional heavy liquid and magnetic separation techniques. Where possible, white mica, apatite, and zircon were also extracted, but the nature of the

samples was not amenable to extraction of these phases in all cases.

[13] Six K-feldspar samples were investigated using  $^{40}\text{Ar}/^{39}\text{Ar}$  analysis, with subsidiary  $^{40}\text{Ar}/^{39}\text{Ar}$  analysis of white mica from two of these (WCG-1 and WCG-2) to ascertain whether they had been isotopically reset during Cenozoic events. The K-feldspar analysis was undertaken in the Nevada Isotope Geochronology Laboratory of the University of Nevada, Las Vegas, Nevada, USA. Samples were irradiated for 10–14 hours at the Texas A&M Nuclear Science Center using Fish Canyon Tuff Sandine, with an age of 27.9 Ma [Steven *et al.*, 1967; Cebula *et al.*, 1986], as a fluence monitor. Corrections for interfering reactions were made using  $\text{CaF}_2$  and K-glass included in the irradiation package. Mass discrimination was monitored by analysis of atmospheric argon from an online pipette. Single crystals of

Table 1. Sample Locality and Lithology Information

Sample	Field Number	Locality	Formation	Lithology	Latitude, °S	Longitude, °E	Elevation, m
FF-10	120100-2	tributary to Doctor Creek	Fraser Fault	cataclasite	42° 57.2'	170° 57.91'	225
FF-9	120100-3	tributary to Doctor Creek	Fraser Complex	granite	42° 57.154'	170° 57.905'	235
WCG-6	140100-3	Geologist Creek	Karamea Intrusive Suite	granite	42° 51.4'	171° 10.8'	180
WCG-4	150100-2	Styx River	Fraser Complex	highly sheared granitic gneiss	42° 53.01'	171° 09.27'	100
WCG-5	170100-6	McPherson Creek	Fraser Complex	sheared granite	42° 48.87'	171° 15.27'	215
WCG-3	200100-1	Whataroa quarry	Karamea Intrusive Suite	foliated granite	43° 16.70'	170° 21.66'	120
WCG-11	200100-2	Whataroa quarry	Karamea Intrusive Suite	foliated granite	43° 16.97'	170° 21.77'	100
WCG-1	270100-1	Arawhata River	intrusion within Greenland Group	granite pegmatite	44° 02.44'	168° 43.00'	20
WCG-2	300100-1	Paringa	Karamea Intrusive Suite	granite	43° 42.74'	169° 27.90'	80
TSG-7	TK-7	Mount Te Kinga	Te Kinga monzogranite	granite	43° 06.54'	170° 52.45'	1200
TSG-8	KFR-7	Mount Te Kinga	Te Kinga monzogranite	granite	43° 07.46'	170° 49.98'	120

standards were loaded into a Cu laser tray and fused with a 20 W CO<sub>2</sub> laser, and step heating was accomplished using a double vacuum resistance furnace. The furnace was calibrated for diffusion experiments using a double thermocouple arrangement (one inside on the crucible base in the sample position, with the control thermocouple in the standard position on the outside of the crucible base). For diffusion calculations the actual temperature-time curve from the inner thermocouple was used. Argon isotopic compositions were measured using a MAP 215-50 rare gas mass spectrometer with a Balzers electron multiplier operated at  $\sim 6.0 \times 10^{-17}$  mol mV<sup>-1</sup> sensitivity. Control of the analysis system and data reduction utilized LabVIEW software written by B. Idleman (Lehigh University). All analytical errors are reported at the 1 $\sigma$  uncertainty level.

[14] Step heating experiments on the white mica samples were performed in the Syracuse University Noble Gas Isotopic Research Laboratory. Purified mica separates were wrapped individually in Sn foil. Samples were vacuum sealed in super-silica quartz tubes along with similarly wrapped packets of biotite age standard GA1550 (97.9 Ma) used to monitor the neutron dose [McDougall and Harrison, 1999] and irradiated for 10 hours in position L-67 of the Ford reactor at the University of Michigan.

[15] Extraction of gas from micas was accomplished using a double-vacuum, resistance-heated tantalum furnace with temperature control via a thermocouple in contact with the bottom of the crucible and mounted on the outer (low) vacuum side of the furnace. Three SAES getters were used for purification of the extracted gas. Isotopic analyses were performed using a VG5400 mass spectrometer with an ion-counting electron multiplier. The mass discrimination and sensitivity of the mass spectrometer (1.499E-4 amps/torr at 100 $\mu$ A trap current) were determined from repeated analysis of atmospheric argon. The extraction line was controlled by a customized LabVIEW program and data reduction done using in-house programs at Syracuse University. Samples were corrected for blanks, neutron-induced interfering isotopes, decay of <sup>37</sup>Ar and <sup>39</sup>Ar, mass discrimination, and atmospheric argon. Correction factors used to account for interfering nuclear reactions were determined by analyzing argon extracted from irradiated CaF<sub>2</sub> and K<sub>2</sub>SO<sub>4</sub>.

[16] All <sup>40</sup>Ar/<sup>39</sup>Ar ages quoted here are calculated using the decay constants recommended by Steiger and Jäger [1977]. Stated precision for these ages includes all uncertainties in the measurement of isotopic ratios and is quoted at the 1 $\sigma$  level. The uncertainties quoted include uncertainty on the J parameter, but not uncertainty in the age of the fluence monitor or the decay constant.

[17] Fission track analysis was carried out at Syracuse University. Apatite grains were mounted in epoxy resin on glass slides, ground and polished to reveal an internal surface, and then etched for 20 s at room temperature in 5N HNO<sub>3</sub> to reveal spontaneous fission tracks. Samples were irradiated at the Oregon State University nuclear reactor in the slow soaker position B-3 (thermal column number 5) that has a Cd for Au ratio of 14 at the column face. Apatite ages were determined using the external detector method, utilizing an automated stage. Mounts were

counted at a magnification of 1250 $\times$  under a dry 100 $\times$  objective. Ages were calculated using the zeta calibration method (zeta = 361  $\pm$  10 for dosimeter glass CN5) following the procedures of Hurford and Green [1983] and Green [1985].

[18] (U-Th)/He dating of apatite samples was done in the (U-Th)/He laboratory at the California Institute of Technology, using the techniques outlined by House *et al.* [1997]. Helium was analyzed by isotope dilution on a Balzers QMG-064 quadrupole mass spectrometer, with outgassed samples extracted from the furnace and dissolved before analysis of U and Th on a Finnegan Element double-focusing ICPMS.

## 5. Data From <sup>40</sup>Ar/<sup>39</sup>Ar Analysis

[19] The advantage of <sup>40</sup>Ar/<sup>39</sup>Ar dating over the conventional K-Ar method is that samples need not be directly fused to release argon, but can instead be outgassed in a sequence of heating steps, starting at temperatures well below that of fusion [McDougall and Harrison, 1999]. The argon extracted at each step can be independently analyzed, providing a series of ages related to the distribution of <sup>40</sup>Ar retention within each individual sample, which can reveal important additional clues to a sample's history.

[20] Step heating analysis is of particular value for K-feldspar, which is anhydrous, and remains stable during heating in vacuo up to the onset of melting. Most of the argon trapped within K-feldspar can thus be driven off in the lab via existing diffusion pathways, allowing experimental determination of diffusion characteristics for each individual sample [Lovera *et al.*, 1991, 1997; Richter *et al.*, 1991]. Such argon diffusion studies [e.g., Lovera *et al.*, 1997, 2002] have demonstrated that most K-feldspars possess diffusion properties (E, the activation energy for motion of the diffusant within the crystal structure, and D<sub>0</sub>/r<sup>2</sup>, the effective diffusion coefficient for the system) that vary as a function of temperature. The most successful explanation of this behavior to date is the multiple diffusion domain (MDD) model of Lovera *et al.* [1989]. The MDD model proposes the presence of a distribution of discrete noninteracting domains in the K-feldspar crystal lattice. This model is able to successfully relate the degassing systematics of reactor-produced <sup>39</sup>Ar<sub>K</sub> observed during laboratory heating to the age spectrum of a sample (reflecting loss and retention of <sup>40</sup>Ar\* on geological time-scales), providing the basis for reconstruction of thermal histories over a broad temperature range ( $\sim 150^{\circ}$ – $350^{\circ}$ C) applicable to the midcrust [Lovera *et al.*, 1989].

[21] The results of <sup>40</sup>Ar/<sup>39</sup>Ar step heat experiments on eight K-feldspar samples are shown in Figure 2. Six of these samples were dated in this study, and detailed analytical data are available from the authors on request. Original analyses of the remaining two, northernmost samples (TSG-7 and TSG-8) are given by Reiners *et al.* [2004].

[22] WCG-1, the southernmost of the samples, is a deformed pegmatite collected near the Arawhata River. As the distribution of ages during outgassing is the fundamental basis for the construction and interpretation of thermal

histories, we will discuss this behavior in some detail. WCG-1 displays a notably staircase-like age spectrum during progressive heating, with apparent ages ranging from a minimum of 6 Ma to Latest Cretaceous ages of ~73 Ma (Figure 2). Although only exhibited between ~5 and 10% cumulative  $^{39}\text{Ar}$  release, the consistency of the 6 Ma minimum age over 3 sequential experimental steps (Figure 2) argues for its significance in respect of the sample's history.

[23] Initially higher ages during early gas release are inconsistent with volume diffusion behavior, and probably indicate the presence of excess argon ( $^{40}\text{Ar}$  from a source other than in-situ decay of  $^{40}\text{K}$  within a sample) in fluid inclusions [Harrison *et al.*, 1994], or taken up at grain margins at low temperatures [Richter *et al.*, 1991]. A second departure from volume diffusive behavior for WCG-1, with elevated ages observed between 10 and 15% gas release is more likely to be due to low-temperature alteration at grain margins or along fractures within the microcline [Lovera *et al.*, 2002]. The ability to distinguish such behavior and discount it in interpretation of the age spectrum is one of the principal advantages of the  $^{40}\text{Ar}/^{39}\text{Ar}$  step heating method, as compared to the conventional K-Ar dating technique.

[24] The age spectrum of neighboring sample WCG-2 from the Paringa region (Figure 2) comprises a more complex “saddle-shaped” pattern, with ages ranging from a minimum of 18 Ma to 63 Ma immediately prior to the onset of melting.

[25] White mica from these two southern-most samples records nothing of the younger history revealed by the K-feldspars (Figure 2). Over the initial 10% of cumulative gas release from mica sample WCG-1, apparent age increases monotonically from a minimum of ~200 Ma to approximately 300 Ma, thereafter describing minor but irregular variation about this level over the remaining 90% of the age spectrum. White mica from sample WCG-2 displays virtually identical behavior (Figure 2), with ages initially at ~190 Ma, climbing steadily over the initial 10% of gas release and then remaining constant at ~320 Ma for the remainder of the outgassing from this sample.

[26] The  $^{40}\text{Ar}/^{39}\text{Ar}$  age spectrum for K-feldspar sample WCG-3 from the Whataroa area (Figure 2) reveals a minimum apparent age of 6 Ma over three sequential experimental steps. Consistent ages of ~7 Ma observed over four subsequent isothermal steps in the early period of gas release mark this out as a further significant age for this sample. These consistent ages are followed by general increase to a peak age of 23 Ma at the onset of melting after 65% of the gas had been extracted from this sample. Subsequent age variation at higher temperatures is influenced by the structural breakdown of the sample during melting, and can be excluded from interpretation of the diffusive age record.

[27] Underlying superficial disturbance during early gas release, the age spectrum of K-feldspar sample WCG-4, collected from an exposure of the Fraser Complex, reveals two persistent age signals, initially at 5 Ma, and subsequently 8 Ma, that together dominate the record of up to 65% of the total gas released.

[28] A similar pattern of ages is observed for a second Fraser Complex sample, WCG-5 collected from McPherson's Creek, with minimum ages again of 5 Ma over three sequential heating steps and a later dominance of consistent 8 Ma ages. This sample is also notable for displaying the youngest overall age record of any sample analyzed in this study, with ages released at high temperature peaking at ~20 Ma.

[29] Although collected only a short distance west of the Fraser Fault in Geologist Creek (Figure 1), the  $^{40}\text{Ar}/^{39}\text{Ar}$  age spectrum of K-feldspar sample WCG-6 displays little correspondence to those of the nearby Fraser Complex samples, lacking the clear dominance of Pliocene ages that so characterizes WCG-4 and WCG-5 (Figure 2). Rather, apparent ages obtained from WCG-6 increase quickly from a minimum of 8 Ma over three isothermal steps early in the outgassing to ~54 Ma at the onset of melting, mimicking the behavior observed for the geographically distant sample WCG-1 (Figure 2).

[30] Sample TSG-7 from the Hohonu Range (Figure 2) displays a staircase  $^{40}\text{Ar}/^{39}\text{Ar}$  age spectrum geometry for K-feldspar, rising from a minimum of 16 Ma up to ~90 Ma prior to the initiation of melting. Over the first three heating steps, the  $^{40}\text{Ar}/^{39}\text{Ar}$  age spectrum of white mica from this sample increases from an initial minimum of ~85 Ma to a consistent plateau at ~100 Ma that dominates the remainder of the experimental gas release [Reiners *et al.*, 2004].

[31] Nearby sample TSG-8, further from the Alpine Fault in the Hohonu Range (Figure 2) displays very similar  $^{40}\text{Ar}/^{39}\text{Ar}$  release characteristics, with a staircase geometry between a minimum of 12 Ma and a pre-melt maximum of ~55 Ma for K-feldspar, and an initial minimum of 76 Ma for white mica, rising to a relatively consistent level of ~95 Ma over the bulk of gas release [Reiners *et al.*, 2004].

## 6. Fission Track Data

[32] Apatite fission track (AFT) ages were determined for four of the granites dated by K-feldspar  $^{40}\text{Ar}/^{39}\text{Ar}$  analysis above, and a further two samples collected from the Fraser Complex but lacking in K-feldspar (Table 2). Apatite grains from this suite of material were generally of poor quality, with abundant dislocations and imperfections making track identification challenging. This problem was especially acute for FF-9 and WCG-5.

[33] Spontaneous fission track counts were low in all the material examined, requiring data to be analyzed using the statistical methods of Brandon *et al.* [1998] for dealing with samples with low spontaneous track densities (Table 2). All six samples pass the chi-square test with probabilities greater than 5%, indicating that each has a concordant grain-age distribution. The low spontaneous track numbers also prevented meaningful statistical analysis of track length variation, restricting interpretation of the thermal history of these samples. We interpret these samples to have been rapidly cooled through the apatite partial annealing zone, a view consistent with the near concordance of AFT ages with slightly higher temperature K-feldspar  $^{40}\text{Ar}/^{39}\text{Ar}$  data

**Table 2.** Apatite Fission Track Analyses<sup>a</sup>

Sample	Number of Grains	STD ( $\times 10^6$ )	FTD ( $\times 10^5$ )	ITD ( $\times 10^6$ )	U, ppm	% Variation	Chi Square, %	Age, Ma
120100-2	15	1.333 (4479)	0.635 (16)	1.974 (497)	19	<1	90	7.8 $\pm$ 2.4
120100-3	25	1.345 (4479)	0.512 (47)	2.515 (2308)	23	61	5	5.0 $\pm$ 0.8
170100-6	26	1.392 (4479)	0.245 (21)	1.976 (1695)	18	<1	36	3.1 $\pm$ 0.8
200100-1	9	1.404 (4479)	0.151 (3)	0.811 (161)	7	<1	92	5.0 $\pm$ 4.4
270100-1	22	1.440 (4479)	0.640 (40)	9.359 (5849)	81	<1	12	1.8 $\pm$ 0.3
300100-1	52	1.464 (4479)	0.150 (23)	1.026 (1569)	9	<1	30	3.9 $\pm$ 1.0

<sup>a</sup>Parentheses enclose number of tracks counted (density). Standard and induced track densities were measured on mica external detectors (geometry factor = 0.5), and fossil track densities were measured on internal mineral surfaces. Fission track ages and confidence intervals are estimated using the binomial algorithm of *Sneyd* [1984] (see explanation by *Brandon et al.* [1998]). The estimated median (50% probability) of the binomial distribution of the grain-age data provides the best estimate of the FT age for a concordant grain-age distribution. This estimate asymptotically converges with the pooled age estimate [*Galbraith and Laslett*, 1985] as the track counts increase. Concordance of grain age distribution is assessed by the chi-square test [*Galbraith*, 1981], which determines the probability that the counted grains belong to a single age population (within Poissonian variation). If the chi-square value is less than 5%, it is likely that the grains counted represent a mixed-age population with real age differences between single grains. All the above calculations were made using the program EXACT\_X2, available at [www.geology.yale.edu/~brandon](http://www.geology.yale.edu/~brandon).

Brackets show number of tracks counted.

Standard and induced track densities measured on mica external detectors ( $g = 0.5$ ) and fossil track densities on internal apatite surfaces.

Ages calculated using the zeta method (361 for glass CN5) and are reported as central ages.

and the lower temperature constraint afforded by apatite (U-Th)/He ages from the same samples.

[34] Four of the five granites analyzed yield AFT ages of 3–4 Ma within the margins of analytical error, with WCG-1 the only granitic sample to notably depart from this value, at 1.8  $\pm$  0.3 Ma. Sample FF-9, a breccia associated with the Fraser Fault itself, was dated at 7.8  $\pm$  2.4 Ma. *Kamp et al.* [1992] collected seven samples in the Fraser Complex, of which 4 yielded sufficient apatite for fission track analysis. Their Fraser Complex AFT ages, from 0.3  $\pm$  0.3 Ma to 2.0  $\pm$  0.3 Ma are much younger than FF-9. However, their AFT ages from west of the Fraser Complex in Tuhua basement are somewhat older and sample FF-9 most likely comprises material from the Tuhua Basement caught up in the fault zone. *Kamp et al.* [1992] also noted a small (1–2 Myr) apparent offset in AFT ages across the Fraser Fault. The contrast of this relatively minor effect of the Fraser Fault on the AFT data with the prominent and distinctive Fraser Complex signature identified in <sup>40</sup>Ar/<sup>39</sup>Ar ages (see above)

suggests that activity on the Fraser Fault may have largely predated fission track closure in these samples.

## 7. (U-Th)/He Data

[35] Six apatite samples were dated by the (U-Th)/He method. Apatite morphologies for sample WCG-2 were pristine and euhedral, but grains from the other five samples were conspicuously rounded to varying degrees. This rounding of apatite is also apparent in petrographic sections, and can thus be identified as a primary feature, and not the result of processing. Inclusions of zircon 1–2  $\mu$ m across were common in all samples, requiring care in the preparation of grains for analysis. A selection of the most intact and euhedral apatite grains present were picked from each sample, and a subset of these optically determined to be free from inclusions was isolated for analysis in multiple-grain aliquots as described above (Table 3). Aliquots were selected with as little variability in size as possible, in order

**Table 3.** Apatite (U-Th)/He Analyses

Sample Number	Aliquot	FT <sup>a</sup>	FT Corrected Age, Ma	1 Sigma Uncertainty <sup>b</sup>	U, ppm	Th, ppm	He, $\eta$ mol/g	Estimated Mass, $\mu$ g	Mean Radius, $\mu$ m	Mean Length, $\mu$ m
FF-10	A	0.72	1.48	0.04	11.39	7.311	0.0760	10.85	43.50	165.00
FF-9	A	0.78	1.82	0.06	16.23	15.01	0.153	49.45	58.09	249.55
	B	0.78	1.76	0.05	18.34	18.00	0.168	41.17	55.80	244.80
WCG-6	A	0.76	1.39	0.04	38.24	37.86	0.271	26.74	52.00	194.00
WCG-4	A	0.73	0.146	0.004	5.826	3.572	0.00385	18.68	42.60	174.60
WCG-5	A	0.81	2.40	0.08	12.91	2.094	0.0901	76.06	67.23	284.22
	B	0.84	2.01	0.07	9.086	1.451	0.0863	84.97	74.33	291.00
WCG-11	A	0.80	3.30	0.11	5.964	0.6556	0.0877	63.09	63.25	238.50
	B	0.83	3.51	0.12	4.216	0.2189	0.0679	72.31	71.07	302.13
WCG-1	A	0.69	2.02	0.06	12.19	1.440	0.0948	7.757	39.43	190.28
WCG-2	A	0.78	3.83	0.12	5.988	5.286	0.117	41.04	56.10	240.30
		0.79	2.66	0.08	5.508	4.431	0.0744	52.80	57.82	265.91

<sup>a</sup>FT represents correction factor for alpha ejection [after *Farley et al.*, 1996].

<sup>b</sup>Errors reflect estimated analytical uncertainty.

to provide maximum uniformity in the application of the correction for alpha ejection. Sample analyses for which significant helium was extracted on re-heating were assumed to be affected by undetected inclusions of more refractory minerals (e.g., zircon), and are not included in the analytical results described in Table 3.

[36] The reported errors represent the estimated replicable precision of the analyses to one standard deviation [Wolf *et al.*, 1996]. Ages are uniformly young and display no clear geographic trends in their variation. Five of the apatite samples yield ages between 1.4 and 3.4 Ma, with WCG-4 representing a notable outlier to the data set, at only  $146 \pm 4$  ka.

## 8. Thermal Histories

[37] Assuming that argon loss during laboratory heating occurs via the same diffusion pathways in feldspar samples as in nature, results of our step heating experiments allow us to constrain the thermal history for each sample. The argon diffusion characteristics for individual feldspar samples are calculated using an iterative least squares fitting process developed by Lovera *et al.* [1989] to fit the observed pattern of Ar release with increasing temperature. With the diffusion properties of a sample constrained in this way, the observed distribution of ages is explicable as a function of temperature variation through time. This relationship is initially investigated through nonlinear iterative  $\chi^2$  fitting [Lovera, 1992; Quidelleur *et al.*, 1997] to explore the statistical limits of thermal constraint. This statistical constraint is refined by further examination of specific thermal histories against this background to obtain an appropriate fit to the sample data and stratigraphic constraints.

[38] For age spectra to reflect the diffusive processes modeled, variation in gas release at different experimental temperatures should reflect corresponding variation in retentivity in nature, so that for slowly cooled samples, age should increase monotonically throughout the experiment. The high ages observed in the lowest temperature portion of the age spectra of WCG-1 fail this requirement, as apparent age subsequently falls to the well-defined minimum of 6 Ma. This behavior is indicative of the presence of excess Ar, or other complicating factors such as outgassing of alteration phases, and this portion of the age spectrum is ignored in the fitting procedure. Likewise, gas extracted above the onset of melting in K-feldspar at  $1100^\circ\text{C}$  is not considered in this modeling, as again, this phenomenon does not reflect diffusion of Ar from feldspars in the geologic environment.

[39] Modeling of experimental results for WCG-1 indicate that this sample was maintained at temperatures of  $\sim 250^\circ\text{C}$  in early Eocene to late Miocene time. This near-isothermal period is required to satisfactorily reproduce the age gradient dominating the age spectrum for this sample between  $\sim 10\%$  and  $55\%$  gas release. The younger ages observed in the first  $10\%$  of gas release then require cooling at rates of  $\sim 20^\circ\text{C}/\text{Ma}$ , beginning no earlier than  $9 \pm 1$  Ma, and with the best fit to the observed age spectrum attained at the earlier end of this range at  $\sim 8.5$  Ma.

[40] The  $^{40}\text{Ar}/^{39}\text{Ar}$  analysis of white mica constrains the higher-temperature history for this sample. Numerical modeling of the available constraint on argon retention and loss in white mica as a function of temperature [Lister and Baldwin, 1996] suggests a closure temperature of approximately  $400^\circ\text{C}$  is appropriate for rapid cooling such as might follow upper crustal emplacement of a granitic magma.

[41] Although step heating of white mica can sometimes yield  $^{40}\text{Ar}/^{39}\text{Ar}$  age spectra with apparent diffusional gradients [McDougall and Harrison, 1999] (i.e., superficially similar to those extracted from analysis of K-feldspar), the thermal significance of these with respect to the geological record is ambiguous, as detailed laboratory studies have demonstrated that argon loss from mica during heating under vacuum is controlled primarily by rates of dehydroxylation and delamination [Sletten and Onstott, 1998]. We consequently choose a cautious approach in interpreting our white mica data, on the basis of the empirical demonstration that white mica commonly yields flat  $^{40}\text{Ar}/^{39}\text{Ar}$  age spectra when rapidly cooled and undisturbed, and apparently sensible age gradients when partially overprinted or slowly cooled [Lanphere and Dalrymple, 1971; Harrison and McDougall, 1981; Wijbrans and McDougall, 1986; Baldwin and Harrison, 1992; Baldwin, 1996].

[42] White mica sample WCG-1 displays such an age gradient (Figure 2). The  $^{40}\text{Ar}/^{39}\text{Ar}$  apparent ages indicate this sample cooled to temperatures at which argon was effectively retained at  $\sim 320$  Ma (Figure 2), while the age gradient across the initial  $10\%$  of argon release is indicative of reheating at  $\sim 180$  Ma to cause minor remobilization of argon [McDougall and Harrison, 1999]. In this section these white micas exhibit reaction rims that also offer an alternative interpretation that the 180 Ma apparent ages may record the timing of partial recrystallization. White mica from sample WCG-2 suggests a similar pattern of cooling to below  $400^\circ\text{C}$  at 300 Ma, with a subsequent overprint at  $\sim 200$  Ma to disturb the spectrum (Figure 2).

[43] It is unclear whether diffusive loss of argon or argon loss due to recrystallization should be the preferred explanation for the observed resetting of argon systematics in these samples. The virtually identical timing observed in the white mica age spectra of both WCG-2 and WCG-1, however, provide confidence that these Devonian and Jurassic mica ages are geologically meaningful. In contrast to the K-feldspar age spectra observed, these white micas do not show evidence for resetting of argon systematics during the Cenozoic.

[44] The age spectrum for K-feldspar sample WCG-2 reveals an age gradient and disturbance of the age spectrum during low-temperature gas release which prevents insight into the post-Miocene history of this sample. This behavior may be linked to low-temperature alteration, with sericitic alteration prominent at grain boundaries and fractures. Despite these potential complications, the high temperature portion of the age spectrum and modeled thermal history mimic that observed for the better-constrained members of

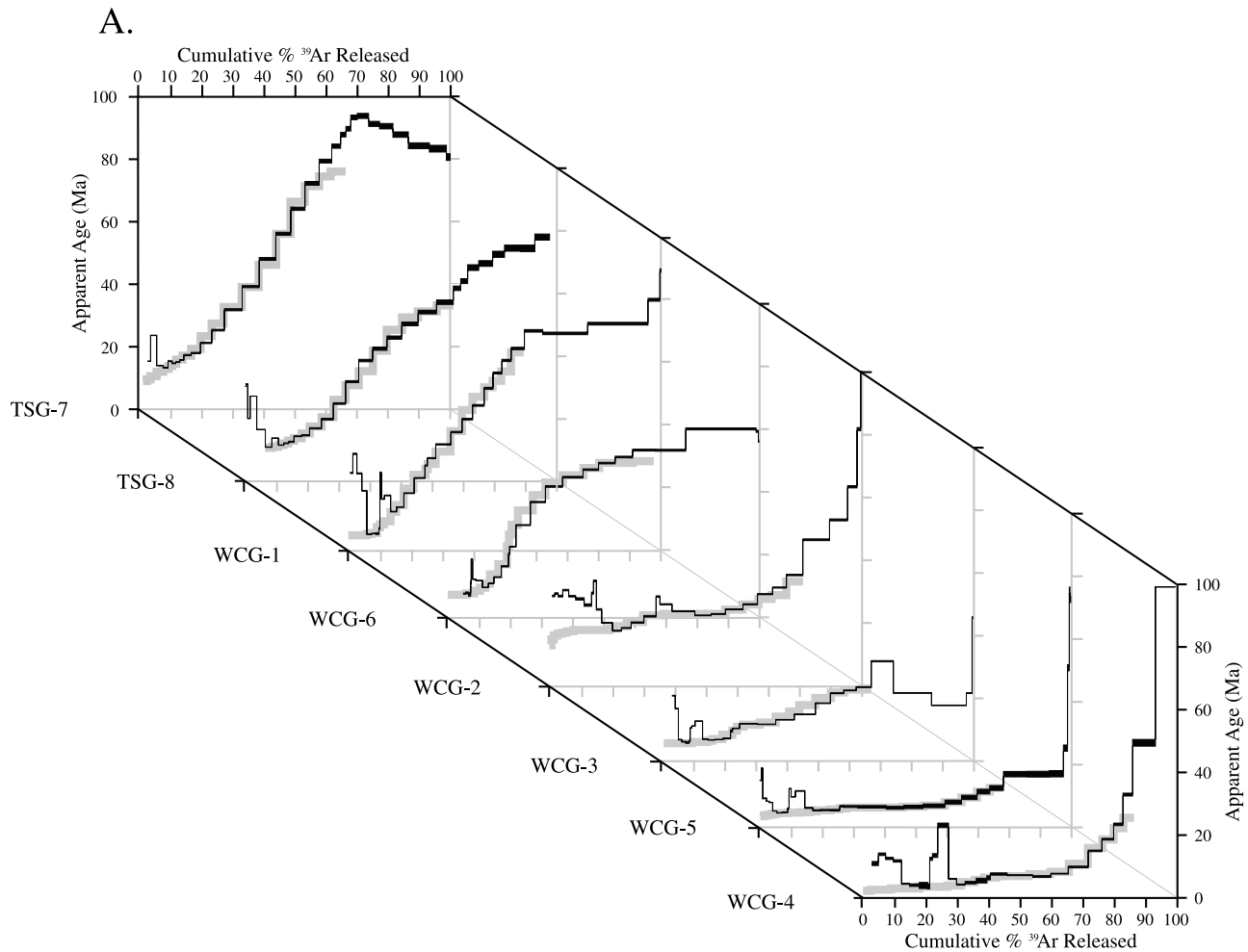


**Figure 3.** Modeled cooling history constraint from thermochronologic data. (a) Comparison of observed K-feldspar  $^{40}\text{Ar}/^{39}\text{Ar}$  age spectra (solid lines; truncated in low-temperature steps for purposes of clarity) with synthetic age spectra resulting from the best fit modeled thermal histories (gray lines). Sample order does not reflect geographic distribution, with curves arranged solely in order to minimize overlap between age spectra and optimize clarity of the figure. (b) Modeled thermal histories of individual samples. Irregular solid and gray envelopes represent 90% confidence intervals for the median (gray) and overall distribution (solid) of modeled cooling histories producing optimum fit to the experimental K-feldspar data. Open rectangles represent apatite fission track constraint, and dark gray rectangles mark apatite (U-Th)/He constraint of temperature.

the sample suite (Figure 3b), and we include the results in this discussion for comparative purposes. Early Miocene ages observed between  $\sim 30$  and 60% cumulative Ar release are best fit by a discrete interval of cooling at  $\sim 10^\circ\text{C}/\text{Ma}$  initiating at  $23 \pm 2$  Ma (Figure 3b).

[45] For K-feldspar sample WCG-3, modeling indicates that the age gradient between  $\sim 15$  and 25 Ma (Figure 3a) results from a short-lived episode of cooling at  $\sim 15^\circ\text{C}/\text{Ma}$  between 25 and 20 Ma and subsequent near-isothermal stability at  $\sim 240^\circ\text{C}$  throughout the remainder of the Miocene and Pliocene. Alternative production of the  $\sim 15$  Ma ages by discrete cooling around this time is rejected, as this produces unacceptable fit to the low temperature portion of the age spectrum. The minimum

ages observed in the first 20% of gas released require marked acceleration of cooling at  $7 \pm 3$  Ma, with best-fit obtained for  $\sim 8$  Ma (Figure 3b).

[46] For K-feldspar WCG-4 (Figure 3a) modeling suggests an episode of cooling from  $\sim 400^\circ$  to  $250^\circ\text{C}$  between 25 and 20 Ma, but constraint on this portion of the age spectrum is relatively poor (Figure 3b). In order to replicate the increase in apparent ages between 60 and 85% of the gas released, the best simulated fit to the observed age spectrum using these diffusion properties requires that cooling of the sample paused at  $\sim 20$  Ma, with the sample subsequently remaining at ambient temperatures of  $200^\circ\text{C}$  for an extended period. The consistent expression of 8 Ma ages and earlier 5 Ma ages during low-

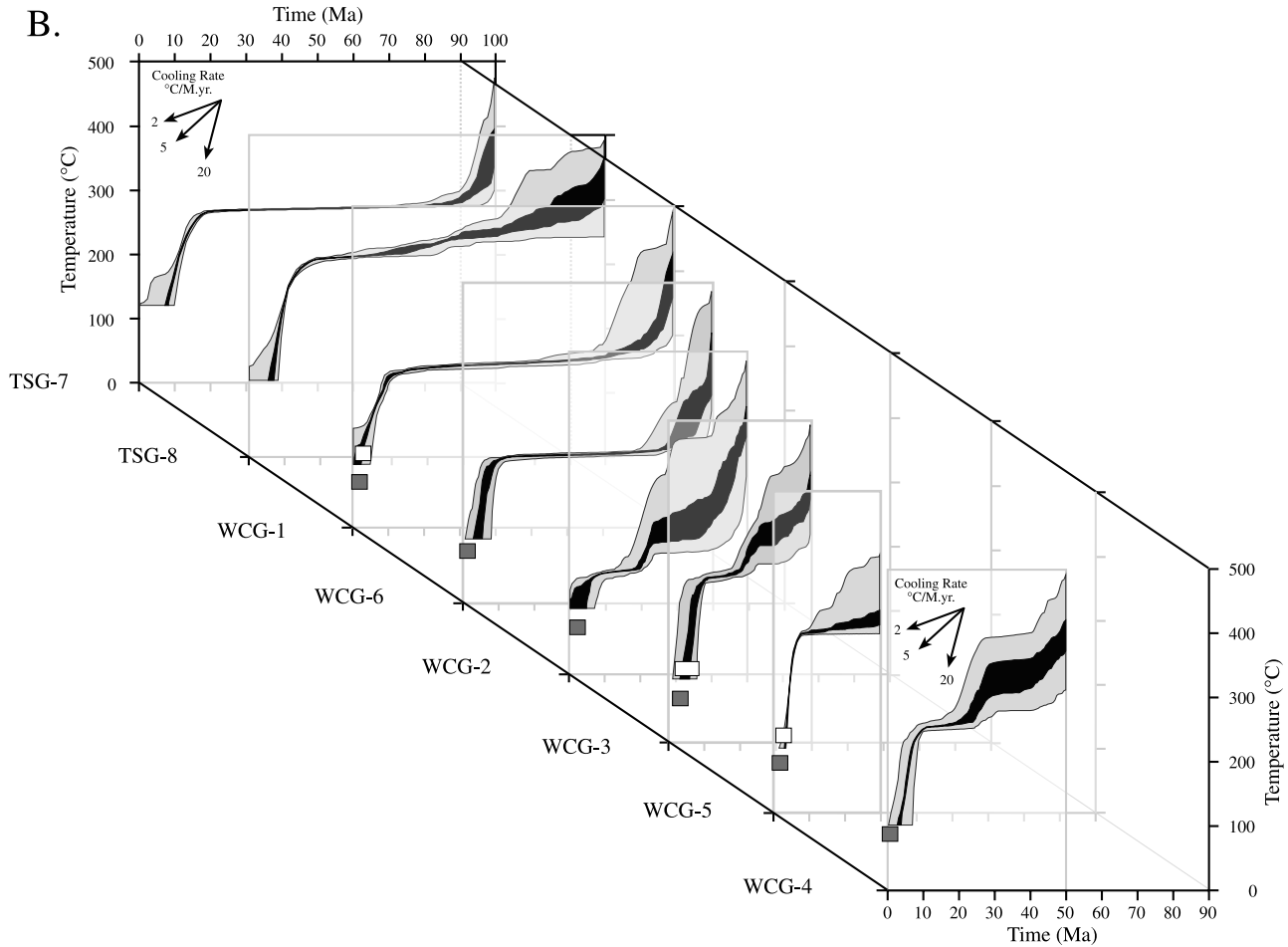


**Figure 3.** (continued)

temperature gas release from this sample (Figure 3a) require renewed acceleration of cooling in the Pliocene. This is modeled as initially occurring at rates of  $\sim 10^{\circ}\text{C}/\text{Ma}$  beginning between 10 and 8 Ma (with best model fit obtained for  $\sim 8.5$  Ma), increasing to  $40^{\circ}\text{C}/\text{Ma}$  over the ensuing 2–3 Ma.

[47] Apparent ages of 5–8 Ma underlying more than 60% of the gas released render WCG-5 particularly important in constraining Pliocene-Recent thermal history. Fitting this age distribution requires rapid cooling of this sample to have initiated at approximately 8 Ma and continued through to the present day, with marked acceleration of cooling over the initial 2–3 Myr of that interval. Pre-Pliocene constraints for this sample are poor, but the increase in age toward higher temperature argon release suggests possible Miocene cooling.

[48] Late Cretaceous cooling of K-feldspar WCG-6 is strongly indicated by gas release in the high temperature portion of the age spectrum, although constraint on the timing of this early cooling is poor. Whatever its precise nature, this cooling ceases as the sample reaches  $\sim 200^{\circ}\text{C}$ , with these consistent ambient temperatures required throughout Paleocene-Pliocene time to model the central

portion of the age spectrum. The minimum ages observed during in the initial 10% of gas released indicate subsequent rapid cooling beginning at  $8 \pm 0.5$  Ma, but disruption of the early spectrum leaves this episode potentially ambiguous.

[49] The simple characteristic staircase geometries of TSG-7 and TSG-8 are best reproduced by very slow to negligible cooling to maintain the K-feldspars at or just below  $300^{\circ}\text{C}$  from the Late Cretaceous through to the Miocene, followed by an increase to  $\sim 20^{\circ}\text{C}/\text{Ma}$  at 15–23 Ma (see *Reiners et al.* [2004] for details).

[50] The thermal significance of the apatite (U-Th)/He data is calculated by iterative solution of the cooling rate-closure temperature relationship using the diffusion model described by *Batt et al.* [2001]. Cooling is assumed to occur at a constant rate between closure of the samples to helium diffusion and surface conditions of  $10^{\circ}\text{C}$ . For the 1.4 to 3.4 Ma apatite (U-Th)/He ages of samples WCG-1, WCG-11, WCG-6, WCG-5, and WCG-2, this procedure yields effective closure temperatures ranging from  $77^{\circ}$ – $82^{\circ}\text{C}$ , offering independent support for the rapid Pliocene-Pleistocene cooling trends indicated by modeling of the K-feldspar  $^{40}\text{Ar}/^{39}\text{Ar}$  data for these samples (Figure 3b).

For the moderate rates of cooling experienced by these samples, the effect of crystal size on (U-Th)/He closure temperature is very small and can effectively be neglected [Reiners and Farley, 2001].

[51] Modeling the  $0.15 \pm 0.01$  Ma (U-Th)/He age of WCG-4 requires a higher effective closure temperature of  $95^{\circ}$ – $105^{\circ}$ C (Figure 3b). The associated rates of cooling are also extremely high, at  $630^{\circ}$ – $700^{\circ}$ C/Ma. An alternative interpretation, given the highly sheared nature of this sample (Table 1) and its proximity to both the Alpine and Fraser Faults (Figure 2), is that the isolated Holocene apatite (U-Th)/He age may indicate resetting by thermal effects of hydrothermal fluids or near-surface shear heating. These possibilities are being explored in continuing work.

[52] Although the scarcity of spontaneous fission tracks prevents their detailed application to constrain thermal history through track length modeling, the apatite fission track ages of these samples provide a useful independent test of the low-temperature thermal histories derived through  $^{40}\text{Ar}/^{39}\text{Ar}$  and (U-Th)/He analysis of these samples (Figure 3b). For the four samples for which this added constraint is available, the AFT data are concordant with the trends of the  $^{40}\text{Ar}/^{39}\text{Ar}$  K-feldspar and apatite (U-Th)/He-derived cooling histories of the respective samples. This integrated data set allows us to define the low temperature cooling histories for these samples with greater confidence, despite complexities in the low temperature portions for some of the K-feldspar  $^{40}\text{Ar}/^{39}\text{Ar}$  age spectra.

## 9. Discussion

[53] The 300–320 Ma apparent ages dominating the white mica age spectra of WCG-1 and WCG-2 provide a link to the Karamea intrusive suite emplaced in the Western Province of the South Island during the Middle to Late Devonian intrusive event identified by Cooper and Tulloch [1992]. We interpret these ages to reflect initial postcrystallization cooling of these minor granitic bodies following their emplacement during this event.

[54] The mid-Jurassic remobilization of argon or minor recrystallization seen in white mica from both of these widely separated samples at  $\sim 180$ – $200$  Ma (Figure 2) is more enigmatic, as this has been argued to be a period of tectonic quiescence in southern New Zealand, with little known orogenic or intrusive activity [e.g., Kimbrough and Tulloch, 1989; Muir et al., 1994, 1996]. Minor basaltic dikes crosscutting WCG-2 at Paringa may offer resolution of this issue. Although heavily altered and undated at present, these later basalts offer the possibility, albeit highly speculative, of association with the Kirwans Dolerite found in northern Westland. This is one of the few intrusive rocks in New Zealand dated to the mid-Jurassic, and has been geochemically correlated with the widespread Ferrar and Tasmanian Dolerite suites [Mortimer et al., 1995], and thus might be expected to have a wider regional expression in the peripheral New Zealand regions of the Jurassic Gondwana margin. Further work on the

$^{40}\text{Ar}/^{39}\text{Ar}$  mica record of the West Coast is underway to test this hypothesis.

[55] Cretaceous  $^{40}\text{Ar}/^{39}\text{Ar}$  mica ages for TSG-7 and TSG-8 suggest the Te Kinga Pluton within the Hohonu Batholith, from which these samples are derived (Table 1) [see Reiners et al., 2004] is a later intrusive body, related to the last of the three main granitic suites on the West Coast, emplaced during the Cretaceous rifting of New Zealand from Australia and Antarctica [Kimbrough and Tulloch, 1989; Seward, 1989; Muir et al., 1994, 1996; Batt et al., 1999] (Figure 4). This is corroborated by a zircon U/Pb age for this pluton of  $108.7 \pm 3.0$  Ma ( $2\sigma$ ) [Waight et al., 1997]. The observation of Cretaceous ages during high temperature breakdown of K-feldspar from WCG-1, WCG-6, and possibly WCG-2 points to possible minor wider-spread regional heating coincident with this intrusive episode.

[56] The principal significance of these new thermochronological results, however, lies in the insight they provide into the Cenozoic development of the AUS-PAC boundary. Rather than offering isolated windows into the evolution of the plate boundary at different times, the direct constraint of our K-feldspar MDD modeling fully spans the Cenozoic history of the region at these selected points close to the plate boundary, in some cases even for individual samples.

[57] Five samples, WCG-4, WCG-3, WCG-2, TSG-7 and TSG-8, record accelerated cooling in the early Miocene (Figures 3b and 4), in each case starting at around 20–25 Ma. For TSG-7 and TSG-8, this cooling episode continues to below the temperature of complete closure for argon in these feldspars, and they consequently offer no constraint on later events. For WCG-2, WCG-3, and WCG-4, however, this cooling ceases in the mid-Miocene before they have attained complete closure. This cessation of cooling is key to the later significance of these samples. By attaining thermal stability within the K-feldspar Ar partial retention zone, they become set up as extremely sensitive indicators of further thermal change; paused on a knife edge between argon retention and loss, they are sensitive to even small changes in temperature. This is reflected in the tightly constrained confidence intervals for these thermal hiatuses.

[58] Significantly, two other widely separated samples, WCG-6 from Geologist Creek near Lake Kaniere in the north of our study area, and WCG-1 from the Arawhata River area in the south, recorded no cooling in the Miocene, despite being highly sensitive to any such thermal change at the time, for the reasons of partial closure discussed above (Figures 3b and 4). Although regionally synchronous then, this activity beginning at 23–25 Ma was apparently localized in its effects, and not universal across the region.

[59] Regional-scale structural reactivation and landscape rejuvenation across the West Coast region at this time is corroborated by the initiation of a short-lived inversion of the Buller Coalfield at 23–24 Ma [Seward, 1989; Kamp et al., 1996], and the sudden influx of voluminous terrigenous sediments of the Inangahua Formation into the

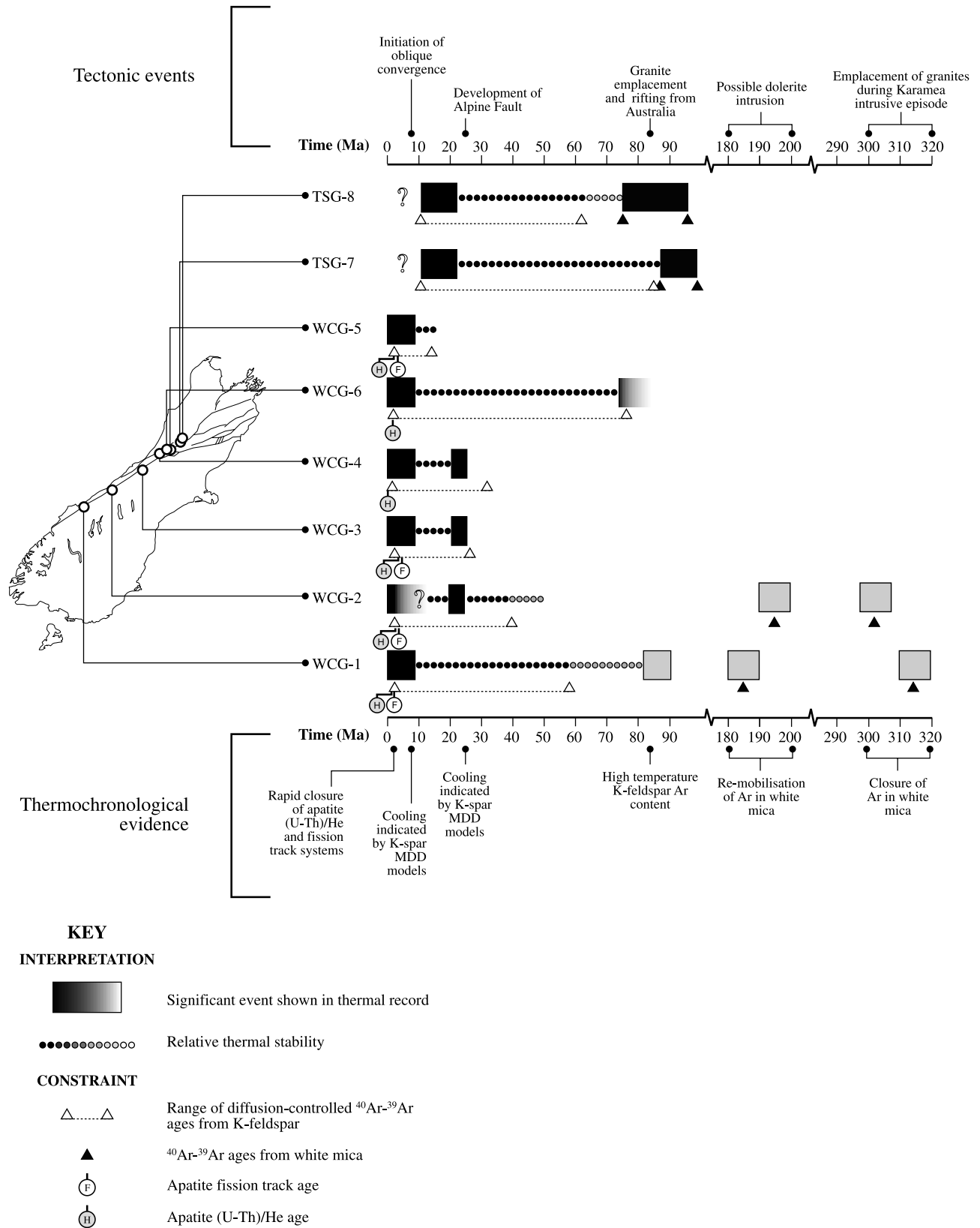


Figure 4. Summary of interpreted constraint on thermotectonic evolution of the analyzed samples.

Inangahua Basin at ~23–24 Ma [Nathan, 1978; Carter *et al.*, 1982].

[60] The timing of this development suggests a link with the initial propagation of the Alpine Fault zone through the South Island as a distributed strike-slip feature linking an earlier series of transtensional basins through the South Island in the early Miocene [e.g., Kamp, 1986; Cooper *et al.*, 1987; King, 2000]. The localized cooling observed may mark uplift and exhumation along misaligned reactivated structures, or at restraining bends or fault segment overlaps across an initially broad zone of deformation. Ongoing investigation of this phenomenon by a more focused study examining spatial variation in thermal history may allow mapping out of these domains. The mid-Miocene cessation of this cooling observed in some samples, and the subsequent thermal hiatus observed, are interpreted to reflect progressive focus of deformation from the initially distributed regional network to specific fault structures which develop primacy, as with the modern dominance of the Alpine Fault. The alternative of a general cessation of tectonic activity can be effectively ruled out, as West Coast basins continue to be supplied with abundant terrigenous sediments throughout the Miocene [Carter *et al.*, 1982].

[61] Perhaps the most striking feature recorded in this study, however, is the abrupt termination of the Miocene cooling hiatus and development of rapid cooling leading up to the present. For the samples best able to constrain the late Miocene-Recent interval (WCG-4 and WCG-5), the onset of this final cooling stage is tightly constrained at ~8 Ma. Thermal models for WCG-1, -3, and -6 are also best fit by accelerated cooling at about this time, although lacking the precision to define the timing precisely (Figure 3b). The other three samples available lack effective resolution of this interval, WCG-2 because of the extensive disruption of the early part of the K-feldspar age spectrum, and TSG-7 and TSG-8 because they had already cooled to below the temperature of complete closure of the Ar system in K-feldspar during the Miocene (Figure 4). This is significant, in that all samples that were sensitive to cooling during the Pliocene period thus appear to converge on a synchronous change in behavior at 8 Ma.

[62] The regional synchronicity of this change and the apparent residence of these samples within the evolving AUS-PAC plate boundary zone lead us to interpret these results with respect to changes in relative AUS-PAC motion. Continuation of the observed rapid cooling through to the present links this change with the onset of the modern regime of oblique convergence across the AUS-PAC boundary, which led in turn to the development of the modern Southern Alps. Major structural inversion at this time is also corroborated by a rapid uplift phase recorded in late Miocene strata in the Brunner-Mount Davy Anticline at around 8 Ma [Kamp *et al.*, 1999], and fission track studies of northern Westland [Kamp *et al.*, 1992] and the Wellington region [Kamp, 2000].

[63] A plate tectonic cause for this event is supported by apparently synchronous Neogene reorganization of

Pacific-North American plate motion. Recently updated calculations of relative plate motion for the Pacific-Antarctic-African-North American plate circuit [Atwater and Stock, 1998] suggest a marked increase in northward motion of the Pacific plate relative to North America at 8 Ma, coincident with changes in extension conditions in the Sierra Nevada and Colorado Plateau.

[64] Although obscured by the already marked cooling ongoing at the time, the prominent 5–6 Ma signal in the low-temperature  $^{40}\text{Ar}/^{39}\text{Ar}$  age spectra of several samples and the corresponding four-fold increase inferred in cooling rates between 8 and 5 Ma (Figure 3b) suggest an extended interval of structural adjustment to the new tectonic regime. Such behavior finds correlative support in the recognition of significant structural readjustment in the Taranaki Basin beginning at ~8 Ma and lasting several Myr [King and Thrasher, 1996; Crowhurst *et al.*, 2002], and in the delay until 5 Ma of major orogenic-linked changes seen in the sedimentary record of some proximal basins [Sutherland, 1996].

[65] Our suggestion of synchronous change in the onshore record differs from the interpretation of Kamp *et al.* [1992], who argued for diachronous development of convergence across the AUS-PAC boundary between 8 Ma in north Westland and 5 Ma in the south. This difference may be a reflection of the contrasting methodologies employed and the corresponding scale of spatial constraint afforded. Whereas we present constraints from individual samples positioned as close as possible to the modern plate boundary to isolate the temporal record of its development, Kamp *et al.* [1992] work in part through the interpolation of spatial trends in geographically widespread data sets collected from the full width of the West Coast. As illustrated by Batt and Brandon [2002], this approach can yield ambiguous results in laterally diverse tectonic settings such as the AUS-PAC boundary zone in the South Island, owing to the superposition of spatial and temporal variation in the thermochronological record.

[66] The 5 Ma signal expressed in several of our age spectra and cooling histories may help to reconcile these views. We have interpreted this signal to indicate extensive structural readjustment to the new plate boundary regime leading up to or at this time, which could thus account for the appearance of the 5 Ma signal so strongly in the wider geographical record investigated by Kamp *et al.* [1992].

## 10. Conclusions

[67] With the exception of TSG-7 and TSG-8, the Westland granites of the AUS plate dated in this study appear to have been intruded to mid or upper crustal levels in the Devonian, leaving them well placed to record subsequent thermal effects resulting from Jurassic and Cretaceous intrusive episodes (including that in which the Te Kinga Pluton was emplaced) and later tectonic developments. In particular, the isotopic record preserved in these samples reveals a multistage regional Cenozoic thermal evolution

that can be related to the development of the AUS-PAC plate boundary. Unlike previous thermochronological investigations of this plate boundary in the South Island of New Zealand, the comprehensive record of Cenozoic thermal events displayed in our samples indicate they have apparently remained strongly influenced by, and presumably in close proximity to, the AUS-PAC plate boundary throughout its progressive evolution.

[68] Regional correlation within our sample set provides constraint of three major thermal changes, which we relate to two distinct periods in the evolution of the AUS-PAC boundary between late Miocene and Recent time. These changes provide key new insight into the evolution of the plate boundary system, as their character and distribution indicate that they are directly attributable to major regional plate tectonic interactions.

[69] The early development of the AUS-PAC plate boundary system through the South Island is recorded as well expressed local cooling as rocks were exhumed to midcrustal levels between ~25 and 20 Ma, tapering off as initially distributed deformation is localized onto a more narrowly defined plate boundary system.

[70] Cessation of Miocene cooling and well-constrained residence of K-feldspar samples at midcrustal temperatures allowing partial diffusive loss of argon [Lister and Baldwin, 1996] provide strong support for tectonic continuity throughout the late Miocene and early Pliocene. This

changes abruptly with the synchronous regional onset of rapid cooling at ~8 Ma. The regional association and character of this event provide a compelling argument to link it with the onset of the modern regime of oblique convergence across the Alpine Fault and the development of the Southern Alps.

[71] The subsequent acceleration of cooling observed for several of our K-feldspar samples between 8 and 5–6 Ma and the correlative delay until 5 Ma of major orogenic-linked sedimentological changes in the West Coast record provide insight into the early constructional period of orogenic development in the system. This inference helps to integrate our revised chronology with the diachroneity observed in the geographically wider-spread studies of Kamp *et al.* [1992] and Sircombe and Kamp [1998], who are able to illustrate the wider regional evolution of the deforming tectonic system away from the proximal effects of the plate boundary.

[72] **Acknowledgments.** This project was supported by National Science Foundation grant EAR- 9909437. M. Cottam was funded by NERC studentship NER/S/A/2000/03588. We are grateful for the logistic and field support provided by Tim Little, Mark Rattenbury, and Victoria and Savannah Aitken over two field seasons. Tod Waight is thanked for supplying samples from the Hohonu Range. We gratefully acknowledge technical support provided by Kathleen Zanetti (UNLV), Laura Webb (SU), and Lindsey Hedges (Caltech). We thank Peter Kamp and two anonymous reviewers for their comments on this manuscript.

## References

- Adams, C. J., and J. E. Gabites (1985), Age of metamorphism and uplift in the Alpine Schist Group at Haast Pass, Lake Wanaka and Lake Hawea, South Island, New Zealand, *N. Z. J. Geol. Geophys.*, **28**, 85–96.
- Allis, R. G. (1986), Mode of crustal shortening adjacent to the Alpine Fault, New Zealand, *Tectonics*, **5**, 15–32.
- Atwater, T., and J. Stock (1998), Pacific-North American plate tectonics of the Neogene southwestern United States—An update, *Int. Geol. Rev.*, **40**, 375–402.
- Baldwin, S. L. (1996), Contrasting P-T-t histories for blueschists from the western Baja Terrane and the Aegean: Effects of synsubduction exhumation and backarc extension, in *Subduction: Top to Bottom, Geophys. Monogr. Ser.*, vol. 96, edited by G. E. Bebout *et al.*, pp. 135–141, AGU, Washington, D. C.
- Baldwin, S. L., and T. M. Harrison (1992), The P-T-t history of blocks in serpentinite-matrix melange, west-central Baja California, *Geol. Soc. Am. Bull.*, **104**, 18–31.
- Batt, G. E. (1997), The crustal dynamics and tectonic evolution of the Southern Alps, New Zealand: Insights from new geochronological data and fully coupled thermo-dynamical finite element modeling, Ph.D. thesis, 273 pp., Aust. Natl. Univ., Canberra, ACT, Australia.
- Batt, G. E. (2001), The approach to steady state thermochronological distribution following orogenic development in the Southern Alps of New Zealand, *Am. J. Sci.*, **301**, 374–384.
- Batt, G. E., and M. T. Brandon (2002), Lateral thinking: 2-D interpretation of thermochronology in convergent orogenic settings, *Tectonophysics*, **349**, 185–201.
- Batt, G. E., and J. Braun (1997), On the thermo-mechanical evolution of compressional orogens, *Geophys. J. Int.*, **128**, 364–382.
- Batt, G. E., and J. Braun (1999), The tectonic evolution of the Southern Alps, New Zealand: Insights from fully thermally coupled dynamical modelling, *Geophys. J. Int.*, **136**, 403–420.
- Batt, G. E., B. P. Kohn, J. Braun, I. McDougall, and T. R. Ireland (1999), New insight into the dynamic development of the Southern Alps, New Zealand, from detailed thermochronological investigation of the Mataketake Range pegmatites, in *Exhumation Processes: Normal Faulting, Ductile Flow and Erosion*, edited by U. Ring *et al.*, *Geol. Soc. Spec. Publ.*, **154**, 261–282.
- Batt, G. E., J. Braun, B. P. Kohn, and I. McDougall (2000), Thermochronological analysis of the dynamics of the Southern Alps, New Zealand, *Geol. Soc. Am. Bull.*, **112**, 250–266.
- Batt, G. E., M. T. Brandon, K. A. Farley, and M. Rodentice (2001), Tectonic synthesis of the Olympic Mountains segment of the Cascadia wedge, using 2-D thermal and kinematic modeling of isotopic age, *J. Geophys. Res.*, **106**, 26,731–26,746.
- Beaumont, C., P. J. J. Kamp, J. Hamilton, and P. Fullsack (1996), The continental collision zone, South Island, New Zealand: Comparison of geodynamical models and observations, *J. Geophys. Res.*, **101**, 3333–3359.
- Brandon, M. T., M. K. Rodentice, and J. I. Garver (1998), Late Cenozoic exhumation of the Cascadia accretionary wedge in the Olympic Mountains, northwest Washington State, *Geol. Soc. Am. Bull.*, **110**, 985–1009.
- Carter, R. M., and R. J. Norris (1976), Cainozoic history of southern New Zealand: An accord between geological observations and plate tectonic predictions, *Earth Planet. Science Lett.*, **31**, 85–94.
- Carter, R. M., J. K. Lindqvist, and R. J. Norris (1982), Oligocene unconformities and nodular phosphate: Hardground horizons in western Southland and northern West Coast, *J. R. Soc. N. Z.*, **12**, 11–46.
- Cebula, G. T., M. J. Kunk, H. H. Mehnert, C. W. Naeser, J. D. Obradovich, and J. F. Sutter (1986), The Fish Canyon Tuff, a potential standard for the <sup>40</sup>Ar-<sup>39</sup>Ar and fission-track dating methods, *Terra Cognita*, **6**, 139–140.
- Chamberlain, C. P., P. K. Zeitler, and A. F. Cooper (1995), Geochronologic constraints of the uplift and metamorphism along the Alpine Fault, South Island, New Zealand, *N. Z. J. Geol. Geophys.*, **38**, 515–523.
- Cooper, A. F. (1979), Petrology of ocellar lamprophyres from Western Otago, New Zealand, *J. Petrology*, **20**, 139–163.
- Cooper, A. F., B. A. Barreiro, D. L. Kimbrough, and J. M. Mattinson (1987), Lamprophyre dike intrusion and the age of the Alpine Fault, New Zealand, *Geology*, **15**, 941–944.
- Cooper, R. A., and G. W. Grindley (Eds.) (1982), Late Proterozoic to Devonian sequences of southeastern Australia, Antarctica and New Zealand and their correlation, *Spec. Publ. Geol. Soc. Aust.*, **9**, 103 pp.
- Cooper, R. A., and A. J. Tulloch (1992), Early Palaeozoic terranes in New Zealand and their relationship to the Lachlan fold belt, *Tectonophysics*, **214**, 129–144.
- Cox, A., and D. C. Engebretson (1985), Change in motion of Pacific plate at 5 Myr BP, *Nature*, **313**, 472–474.
- Crowhurst, P. V., P. F. Green, and P. J. J. Kamp (2002), Appraisal of (U-Th)/He thermochronology as a thermal history tool for hydrocarbon exploration: An example from the Taranaki Basin, New Zealand, *AAPG Bull.*, **86**, 1801–1819.
- Davey, F. J., T. Henyey, S. Kleffman, A. Melhuish, D. Okaya, T. A. Stern, and D. J. Woodward (1995), Crustal reflections from the Alpine Fault Zone, South Island, New Zealand, *N. Z. J. Geol. Geophys.*, **38**, 601–604.

- DeMets, C. G., R. G. Gordon, D. F. Argus, and S. Stein (1990), Current plate motions, *Geophys. J. Int.*, *101*, 425–478.
- Farley K. A., R. A. Wolf, and L. T. Silver (1996), The effects of long alpha-stopping distances on (U-Th)/He ages, *Geochim. Cosmochim. Acta*, *60*, 4223–4229.
- Galbraith, R. F. (1981), On statistical models for fission track counts, *J. Int. Assoc. Math. Geol.*, *13*, 471–478.
- Galbraith, R. F., and G. M. Laslett (1985), Some remarks on statistical estimation in fission-track dating, *Nucl. Tracks Radiat. Measure.*, *10*, 361–363.
- Green, P. F. (1985), Comparison of zeta calibration baselines for fission-track dating of apatite, zircon and sphene, *Chem. Geol.*, *58*, 1–22.
- Harbert, W. (1991), Late Neogene relative motions of the Pacific and North America plates, *Tectonics*, *10*, 1–15.
- Harrison, T. M., and I. McDougall (1981), Excess  $^{40}\text{Ar}$  in metamorphic rocks from Broken Hill, New South Wales: Implications for  $^{40}\text{Ar}/^{39}\text{Ar}$  age spectra and the thermal history of the region, *Earth Planet. Sci. Lett.*, *55*, 123–149.
- Harrison, T. M., M. T. Heizler, O. M. Lovera, W. Chen, and M. Grove (1994), A chlorine disinfectant for excess argon released from K-feldspar during step heating, *Earth Planet. Sci. Lett.*, *123*, 95–104.
- Harrison, T. M., M. Grove, O. M. Lovera, and E. J. Catlos (1998), A model for the origin of Himalayan anatexis and inverted metamorphism, *J. Geophys. Res.*, *103*, 27,017–27,032.
- House, M. A., B. P. Wernicke, K. A. Farley, and T. A. Dumitru (1997), Cenozoic thermal evolution of the central Sierra Nevada, California, from (U-Th)/He thermochronometry, *Earth Planet. Sci. Lett.*, *151*, 167–179.
- Hurfurd, A. J., and P. F. Green (1983), The zeta age calibration of fission-track dating, *Chem. Geol.*, *41*, 285–317.
- Jamieson, R. A., C. Beaumont, J. Hamilton, and P. Fullsack (1996), Tectonic assembly of inverted metamorphic sequences, *Geology*, *24*, 839–842.
- Kamp, P. J. J. (1986), The mid-Cenozoic Challenger Rift System of western New Zealand and its implications for the age of the Alpine Fault, *Geol. Soc. Am. Bull.*, *97*, 255–281.
- Kamp, P. J. J. (1991), Late Oligocene Pacific-wide tectonic event, *Terra Nova*, *3*, 65–69.
- Kamp, P. J. J. (1997), Paleogeothermal gradient and deformation style, Pacific front of the Southern Alps orogen: Constraints from fission track thermochronology, *Tectonophysics*, *271*, 37–58.
- Kamp, P. J. J. (2000), Thermochronology of the Torlesse accretionary complex, Wellington, New Zealand, *J. Geophys. Res.*, *105*, 19,253–19,272.
- Kamp, P. J. J., P. F. Green, and S. H. White (1989), Fission track analysis reveals character of collisional tectonics in New Zealand, *Tectonics*, *8*, 169–195.
- Kamp, P. J. J., P. F. Green, and J. M. Tippet (1992), Tectonic architecture of the mountain front-foreland basin transition, South Island, New Zealand, assessed by fission track analysis, *Tectonics*, *11*, 98–113.
- Kamp, P. J. J., K. S. Webster, and S. Nathan (1996), Thermal history analysis by integrated modelling of apatite fission track and vitrinite reflectance data: Application to an inverted basin (Buller Coalfield, New Zealand), *Basin Res.*, *8*, 383–402.
- Kamp, P. J. J., I. W. Whitehouse, and J. Newman (1999), Constraints on the thermal and tectonic evolution of Greymouth Coalfield, *N. Z. J. Geol. Geophys.*, *42*, 447–467.
- Kimbrough, D. L., and A. J. Tulloch (1989), Early Cretaceous age of orthogneiss from the Charleston Metamorphic Group, New Zealand, *Earth Planet. Sci. Lett.*, *95*, 130–140.
- King, P. R. (2000), Tectonic reconstructions of New Zealand 40 Ma to the present, *N. Z. J. Geol. Geophys.*, *43*, 611–638.
- King, P. R., and G. P. Thrasher (1996), *Cretaceous-Cenozoic Geology and Petroleum Systems of the Taranaki Basin, New Zealand*, 243 pp., Inst. Geol. Nucl. Sci., Lower Hutt, New Zealand.
- Koons, P. O., R. J. Norris, D. Craw, and A. F. Cooper (2003), Influence of exhumation on the structural evolution of transpressional plate boundaries: An example from the Southern Alps, New Zealand, *Geology*, *31*, 3–6.
- Lanphere, M. A., and G. B. Dalrymple (1971), A test of the  $^{40}\text{Ar}/^{39}\text{Ar}$  age spectrum on some terrestrial materials, *Earth Planet. Sci. Lett.*, *12*, 359–372.
- Lister, G. S., and S. L. Baldwin (1996), Modelling the effect of arbitrary P-T-t histories on argon diffusion in minerals using the MacArgon program for the Apple Macintosh, *Tectonophysics*, *253*, 83–109.
- Lovera, O. M. (1992), Computer programs to model  $^{40}\text{Ar}/^{39}\text{Ar}$  diffusion data from multi-domain samples, *Comput. Geosci.*, *18*, 789–813.
- Lovera, O. M., F. M. Richter, and T. M. Harrison (1989), The  $^{40}\text{Ar}/^{39}\text{Ar}$  thermochronometry for slowly cooled samples having a distribution of diffusion domain sizes, *J. Geophys. Res.*, *94*, 17,935–19,917.
- Lovera, O. M., F. M. Richter, and T. M. Harrison (1991), Diffusion domains determined by  $^{39}\text{Ar}$  released during step heating, *J. Geophys. Res.*, *96*, 2057–2069.
- Lovera, O. M., M. Grove, T. M. Harrison, and K. I. Mahon (1997), Systematic analysis of K-feldspar  $^{40}\text{Ar}/^{39}\text{Ar}$  step heating results; I, Significance of activation energy determinations, *Geochim. Cosmochim. Acta*, *61*, 3171–3192.
- Lovera, O. M., M. Grove, and T. M. Harrison (2002), Systematic analysis of K-feldspar  $^{40}\text{Ar}/^{39}\text{Ar}$  step heating results; II, Relevance of laboratory argon diffusion properties to nature, *Geochim. Cosmochim. Acta*, *66*, 1237–1255.
- McDougall, I., and T. M. Harrison (1999), *Geochronology and Thermochronology by the  $^{40}\text{Ar}/^{39}\text{Ar}$  Method*, 2nd ed., 269 pp., Oxford Univ. Press, New York.
- Molnar, P., T. Atwater, J. Mammerickx, and S. M. Smith (1975), Magnetic anomalies, bathymetry and the tectonic evolution of the South Pacific since the Late Cretaceous, *Geophys. J. R. Astron. Soc.*, *40*, 383–420.
- Mortimer, N., D. Parkinson, J. I. Raine, C. J. Adams, I. J. Graham, P. J. Oliver, and K. Palmer (1995), Ferrar magmatic province rocks discovered in New Zealand: Implications for Mesozoic Gondwana geology, *Geology*, *23*, 185–188.
- Muir, R. J., T. R. Ireland, S. D. Weaver, and J. D. Bradshaw (1994), Ion microprobe U-Pb zircon geochronology of granitic magmatism in the Western Province of the South Island, New Zealand, *Chem. Geol.*, *113*, 171–189.
- Muir, R. J., T. R. Ireland, S. D. Weaver, and J. D. Bradshaw (1996), Ion microprobe dating of Paleozoic granitoids: Devonian magmatism in New Zealand and correlations with Australia and Antarctica, *Chem. Geol.*, *127*, 191–210.
- Nathan, S. (1975), Stratigraphic classification and nomenclature in Buller and North Westland: Reply, *N. Z. J. Geol. Geophys.*, *18*, 642–649.
- Nathan, S. (1978), Upper Cenozoic stratigraphy of South Westland, New Zealand, *N. Z. J. Geol. Geophys.*, *21*, 329–361.
- Nathan, S., H. J. Anderson, R. A. Cook, R. H. Herzer, R. H. Hoskins, J. I. Raine, and D. Smale (1986), *Cretaceous and Cenozoic Basins of the West Coast Region, South Island, N. Z. Geol. Surv. Basin Stud.*, vol. 1., 90 pp., N. Z. Geol. Surv., Wellington.
- Norris, R. J., and A. F. Cooper (2001), Late Quaternary slip rates and slip partitioning on the Alpine Fault, New Zealand, *J. Struct. Geol.*, *23*, 507–520.
- Norris, R. J., P. O. Koons, and A. F. Cooper (1990), The obliquely convergent plate boundary in the South Island of New Zealand: Implications for ancient collision zones, *J. Struct. Geol.*, *12*, 715–725.
- Pearson, C. F., J. Beavan, D. J. Darby, G. H. Blick, and R. I. Walcott (1995), Strain distribution across the Australian-Pacific plate boundary in the central South Island, from 1992 GPS and earlier terrestrial observations, *J. Geophys. Res.*, *100*, 22,071–22,081.
- Pollitz, F. (1986), Pliocene changes in Pacific plate motion, *Nature*, *320*, 738–741.
- Quidelleur, X., M. Grove, O. M. Lovera, T. M. Harrison, A. Yin, and F. J. Ryerson (1997), Thermal evolution and slip history of the Renbu Zedong Thrust, southeastern Tibet, *J. Geophys. Res.*, *102*, 2659–2679.
- Rattenbury, M. S. (1987), Timing of mylonitisation west of the Alpine Fault, central Westland, New Zealand, *N. Z. J. Geol. Geophys.*, *30*, 287–297.
- Reed, J. J. (1958), Regional metamorphism of southeast Nelson, *N. Z. Geol. Surv. Bull.*, *60*, 64 pp.
- Reyners, M., and H. Cowan (1993), The transition from subduction to continental collision: Crustal structure in the North Canterbury region, New Zealand, *Geophys. J. Int.*, *115*, 1124–1136.
- Reiners, P. W., and K. A. Farley (2001), Influence of crystal size on apatite (U-Th)/He thermochronology: An example from the Bighorn Mountains, Wyoming, *Earth Planet. Sci. Lett.*, *188*, 413–420.
- Reiners, P. W., T. L. Spell, S. Nicolescu, and K. A. Zanetti (2004), Zircon (U-Th)/He thermochronometry: He diffusion and comparisons with  $^{40}\text{Ar}/^{39}\text{Ar}$  dating, *Geochim. Cosmochim. Acta.*, in press.
- Richter, F. M., O. M. Lovera, T. M. Harrison, and P. Copeland (1991), Tibetan tectonics from  $^{40}\text{Ar}/^{39}\text{Ar}$  analysis of a single K-feldspar sample, *Earth Planet. Sci. Lett.*, *105*, 266–278.
- Seward, D. (1989), Cenozoic basin histories determined by fission-track dating of basement granites, South Island, New Zealand, *Chem. Geol.*, *79*, 31–48.
- Shelley, D. (1970), The structure and petrography of the Constant gneiss near Charleston, south-west Nelson, *N. Z. J. Geol. Geophys.*, *13*, 370–391.
- Shi, Y., R. Allis, and F. Davey (1996), Thermal modelling of the Southern Alps, New Zealand, *Pure Appl. Geophys.*, *146*, 469–501.
- Sircombe, K. N., and P. J. J. Kamp (1998), The South Westland Basin: Seismic stratigraphy, basin geometry and evolution of a foreland basin within the Southern Alps collision zone, New Zealand, *Tectonophysics*, *300*, 359–387.
- Sletten, V. W., and T. C. Onstott (1998), The effect of the instability of muscovite during in vacuo heating on  $^{40}\text{Ar}/^{39}\text{Ar}$  step-heating spectra, *Geochim. Cosmochim. Acta*, *62*, 123–141.
- Smith, E. G. C., T. A. Stern, and B. O'Brien (1995), A seismic velocity profile across the central South Island, New Zealand, from explosion data, *N. Z. J. Geol. Geophys.*, *38*, 565–570.
- Sneyd, A. D. (1984), A computer program for calculating exact confidence intervals for age in fission-track dating, *Comput. Geosci.*, *10*, 339–345.
- Steiger, R. H., and E. Jäger (1977), Subcommittee on geochronology: convention on the use of decay constants in geo- and cosmochronology, *Earth Planet. Sci. Lett.*, *36*, 359–362.
- Steven, T. A., H. H. Mehnert, and J. D. Obradovich (1967), Age of volcanic activity in the San Juan Mountains, Colorado, *U. S. Geol. Surv. Prof. Pap.*, *575-D*, 47–55.
- Stüwe, K., L. White, and R. Brown (1994), The influence of eroding topography on steady-state isotherms: Application to fission track analysis, *Earth Planet. Sci. Lett.*, *124*, 63–74.
- Sutherland, R. (1994), Displacement since the Pliocene along the southern section of the Alpine Fault, New Zealand, *Geology*, *22*, 327–330.
- Sutherland, R. (1995), The Australia-Pacific boundary and Cenozoic plate motions in the SW Pacific: Some constraints from Geosat data, *Tectonics*, *14*, 819–831.
- Sutherland, R. (1996), Transpressional development of the Australia-Pacific boundary through southern South Island, New Zealand: Constraints from Miocene-Pliocene sediments, Waiho-1 borehole, South Westland, *N. Z. J. Geol. Geophys.*, *39*, 251–264.

- Sutherland, R., F. Davey, and J. Beavan (2000), Plate boundary deformation in South Island, New Zealand, is related to inherited lithospheric structure, *Earth Planet. Sci. Lett.*, *177*, 141–151.
- Tippett, J. M., and P. J. J. Kamp (1993), Fission track analysis of the late Cenozoic vertical kinematics of continental Pacific Crust, South Island, New Zealand, *J. Geophys. Res.*, *98*, 16,119–16,148.
- Tulloch, A. J. (1983), Granitoid rocks of New Zealand: A brief review, in *Circum-Pacific Plutonic Terranes*, edited by J. A. Roddick, *Mem. Geol. Soc. Am.*, *159*, 5–20.
- Waight, T. E., S. D. Weaver, T. R. Ireland, R. Maas, R. J. Muir, and D. Shelley (1997), Field characteristics, petrography, and geochronology of the Hohonu Batholith and the adjacent Granite Hill Complex, North Westland, New Zealand, *N. Z. J. Geol. Geophys.*, *40*, 1–17.
- Walcott, R. I. (1978), Present tectonics and late Cenozoic evolution of New Zealand, *Geophys. J. R. Astron. Soc.*, *52*, 137–164.
- Walcott, R. I. (1984), Reconstructions of the New Zealand region for the Neogene, *Palaeogeogr. Palaeoclimatol. Palaeoecol.*, *46*, 217–231.
- Walcott, R. I. (1998), Modes of oblique compression: Late Cenozoic tectonics of the South Island of New Zealand, *Rev. Geophys.*, *36*, 1–26.
- White, S. H., and P. F. Green (1986), Tectonic development of the Alpine fault zone, New Zealand: A fission track study, *Geology*, *14*, 124–127.
- Wijbrans, J. R., and I. McDougall (1986),  $^{40}\text{Ar}/^{39}\text{Ar}$  dating of white micas from an Alpine high-pressure metamorphic belt on Naxos (Greece): The resetting of the argon isotopic system, *Contrib. Mineral. Petrol.*, *93*, 187–194.
- Wolf, R. A., K. A. Farley, and L. T. Silver (1996), Helium diffusion and low-temperature thermochronometry of apatite, *Geochim. Cosmochim. Acta*, *60*, 4231–4240.

---

S. L. Baldwin and P. G. Fitzgerald, Department of Earth Sciences, Syracuse University, Syracuse, NY 13244-1070, USA.

G. E. Batt and M. Cottam, Geology Department, Royal Holloway University of London, Surrey TW20 0EX, UK. (g.batt@gl.rhul.ac.uk)

M. T. Brandon, Department of Geology and Geophysics, Yale University, P.O. Box 208109, New Haven, CT 06520-8109, USA.

T. L. Spell, Department of Geoscience, University of Nevada, MS 4010, Las Vegas, NV 89154-4010, USA.